

Boosting SAM for Cross-Domain Few-Shot Segmentation via Conditional Point Sparsification

Jiahao Nie ^{*1,2} Yun Xing ^{*1} Wenbin An ³ Qingsong Zhao ² Jiawei Shao ²
 Yap-Peng Tan ^{4,1} Alex C. Kot ¹ Shijian Lu ¹ Xuelong Li ^{†2}

Abstract

Motivated by the success of the Segment Anything Model (SAM) in promptable segmentation, recent studies leverage SAM to develop training-free solutions for few-shot segmentation, which aims to predict object masks in the target image based on a few reference exemplars. These SAM-based methods typically rely on point matching between reference and target images and use the matched dense points as prompts for mask prediction. However, we observe that dense points perform poorly in Cross-Domain Few-Shot Segmentation (CD-FSS), where target images are from the medical or satellite domain. We attribute this issue to large domain shifts that disrupt the point–image interactions learned by SAM, and find that point density plays a crucial role under such conditions. To address this challenge, we propose Conditional Point Sparsification (CPS), a training-free approach that adaptively guides SAM interactions for cross-domain images based on reference exemplars. Leveraging ground-truth masks, the reference images provide reliable guidance for adaptively sparsifying dense matched points, enabling more accurate segmentation results. Extensive experiments demonstrate that CPS outperforms existing training-free SAM-based methods across diverse CD-FSS datasets.

1. Introduction

Trained on billions of prompt-image-mask triplets, the Segment Anything Model (SAM) (Kirillov et al., 2023) demonstrates unprecedented segmentation capability across diverse objects and granularities. Its promptable segmentation ca-

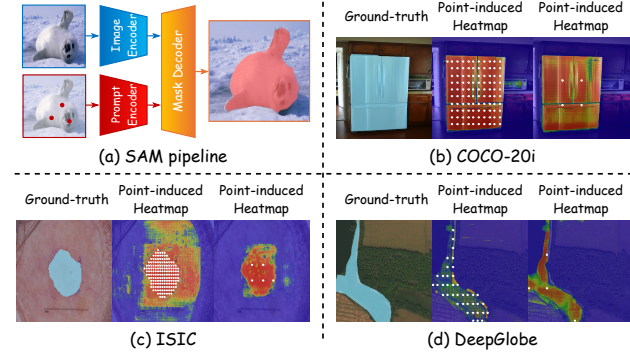


Figure 1. (a) Overview of SAM for promptable segmentation. (b–d) Existing methods exhibit inconsistent segmentation behavior between in-domain and cross-domain images.

pability has enabled a wide range of applications, including automated mask annotation (Zhang et al., 2025; Wang et al., 2023), robotics (Fang et al., 2025; Pan et al., 2025), and virtual reality (Yang et al., 2025). Motivated by SAM’s strong ability to segment prompt-specified objects using prompt points (see Fig. 1(a)), recent works (Liu et al., 2023; Zhang et al., 2024) have explored training-free SAM-based methods for Few-Shot Segmentation, a task that aims to segment target objects conditioned on a few reference exemplars (Wang et al., 2019; Zhang et al., 2019b). These methods typically locate prompt points in the target images via dense matching with the reference images and then use these points as SAM prompts to segment the target objects.

Although existing methods perform well on in-domain datasets (e.g., COCO-20i (Nguyen & Todorovic, 2019)) (Liu et al., 2023), we observe significant performance degradation when they are directly applied to Cross-Domain Few-Shot Segmentation (CD-FSS) datasets, such as medical (Codella et al., 2019; Tschandl et al., 2018) and satellite images (Demir et al., 2018). As shown in Fig. 1(b–d), even when the dense prompt points consistently fall within the target regions (i.e., refrigerator, skin nevus, and water area), the segmentations for skin nevus and water area remain noticeably less accurate. More illustrative examples are provided in the appendix.

We attribute these phenomena to significant domain shifts that disrupt the learned point–image interactions in SAM. Fig. 2 shows t-SNE (Maaten & Hinton, 2008) visualiza-

^{*}Equal contribution [†]Corresponding author

¹Nanyang Technological University ²Institute of Artificial Intelligence (TeleAI), China Telecom ³Xi'an Jiaotong University ⁴VinUniversity. Correspondence to: Jiahao Nie <jiahao007@e.ntu.edu.sg>, Xuelong Li <xuelong_li@ieee.org>.

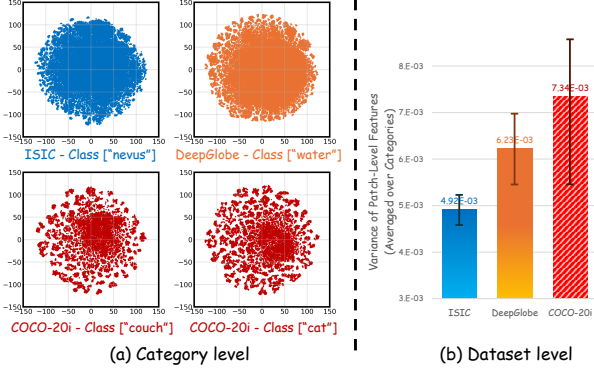


Figure 2. Analysis of SAM-encoded target-object patch features. (a) Category level: t-SNE visualization shows that in-domain images exhibit larger intra-category variance than cross-domain images. (b) Dataset level: Mean variance of all categories (bars) and inter-category variance range (error bars) confirm this trend.

tions of target object features extracted by the SAM vision encoder, revealing clear distribution differences across datasets. We observe that the intra-object feature variance in medical and satellite images is considerably lower than that in COCO-20i. This is consistent with dataset characteristics: objects such as *skin nevus* and *water area* exhibit more uniform and homogeneous semantics, whereas an object like *cat* contains diverse parts (*e.g.*, *head*, *leg*, and *tail*). Moreover, objects in in-domain datasets typically have more complex shapes (Lang et al., 2023), for which dense points are used during SAM training to provide precise spatial guidance. However, when transferred to cross-domain scenarios, such dense points become less suitable and introduce ambiguity: the more homogeneous semantics of these objects require fewer but more informative points. As illustrated in Fig. 1(b–d), sparse points can therefore produce more accurate region activations in these cases. Additional examples are provided in the appendix.

To address the above limitations and extend SAM-based solutions to CD-FSS, we propose Conditional Point Sparsification (CPS), a novel training-free framework that leverages reference exemplars to guide prompt points in the target image. Our approach is grounded in a key observation (Fig. 1(c–d)) that sparse points lead to more reliable SAM interactions, whereas the dense prompts used in existing methods often degrade performance in cross-domain scenarios. Specifically, CPS infers an appropriate point density from few-shot reference exemplars with ground-truth masks, and utilizes this reference density to sparsify the matched points. This conditional sparsification strategy aligns point density with dataset characteristics, thereby improving point–image interactions under domain shifts. Despite its simplicity, CPS consistently outperforms prior SAM-based FSS methods (*e.g.*, Matcher (Liu et al., 2023)) across four cross-domain benchmarks with only lightweight modifications, and also surpasses heuristic sparsification schemes based on manually defined hyperparameters.

The contributions of this work can be summarized in three aspects: *First*, we reveal that the performance degradation of existing SAM-based FSS methods in cross-domain images stems from domain shifts that break the learned point–image interactions in SAM. *Second*, we propose Conditional Point Sparsification (CPS), a simple yet effective training-free strategy that infers appropriate prompt density from few-shot reference exemplars and adopts it to sparsify the matched points in target images. *Third*, CPS improves performance over prior SAM-based training-free approaches across challenging cross-domain benchmarks.

2. Related Work

Cross-Domain Few-Shot Segmentation (CD-FSS) aims to segment target objects conditioned on a few reference exemplars under significant domain shifts (Lu et al., 2021; Boudiaf et al., 2021; Wang et al., 2022; Tong et al., 2025; Wu et al., 2024; Chen et al., 2024b;a). Early works (Lei et al., 2022; Fu et al., 2024; Nie et al., 2024) typically adopt a two-stage paradigm, where an ImageNet (Deng et al., 2009) pre-trained model is first trained on a large-scale source domain and then adapted to each target domain. These methods explore dynamic adaptation, refinement (Fan et al., 2023), knowledge transfer (Huang et al., 2023), feature frequency disentanglement (Tong et al., 2024a), and lightweight structural adaptation (Fan et al., 2025; Su et al., 2024), but still suffer from limited generalization under severe domain shifts. With the advent of visual foundation models (Kirillov et al., 2023; Oquab et al., 2023; Rombach et al., 2022; Ravi et al., 2024), several works (Yang et al., 2024; He et al., 2024; Zhu et al., 2024; Sun et al., 2024; Cuttano et al., 2025; Xu et al., 2025) leverage SAM’s zero-shot and promptable segmentation capability to tackle CD-FSS. However, most of these approaches still rely on training stages, introducing additional computational overhead (Liu et al., 2023; Zhang et al., 2024; Herzog, 2024). In contrast, our work focuses on a training-free solution that no longer relies on domain-specific data for CD-FSS.

SAM Adaptation for Downstream Tasks is an under-explored problem, although SAM excels in dealing with in-domain images such as COCO (Lin et al., 2014). It is well recognized that SAM needs adaptations for downstream tasks, such as medical (Chen et al., 2023; Mazurowski et al., 2023; Ma et al., 2024; Wu et al., 2025) or satellite images (Li et al., 2025; Yan et al., 2023; Ding et al., 2024; Liu et al., 2025), given the significant domain differences between SAM training data and these images. Early approaches involve the collection of large-scale labeled data in a wide spectrum of imaging modalities (Ma et al., 2024) for adaptation, which is expensive and could bring privacy concerns for practical use. Motivated by the strong capability of recent vision foundation models (Oquab et al., 2023; Kirillov et al., 2023; Ravi et al., 2024), more studies explore efficient

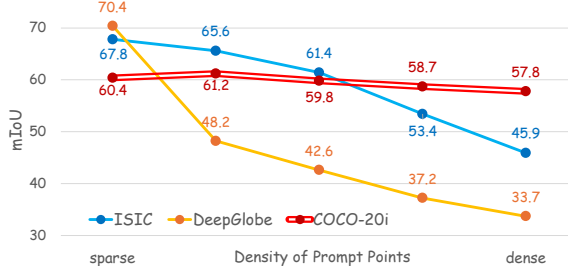


Figure 3. Cross-domain and in-domain datasets exhibit varying sensitivities to prompt point density.

adaptation of SAM to these downstream tasks, with either lightweight architectural add-ons (Chen et al., 2023; Ke et al., 2023) or few-shot samples from data perspective (Xiao et al., 2024a;b). In light of few-shot SAM pipeline for in-domain images (Zhang et al., 2023; Cuttano et al., 2025), we propose a strategy that reduces the need for large-scale or few-shot tuning, enabling cross-domain image segmentation using a few reference exemplars at inference time.

3. Motivation and Preliminary

3.1. Visual Foundation Models

We briefly introduce two visual foundation models adopted in this paper, *i.e.*, DINOv2 (Oquab et al., 2023) and SAM (Kirillov et al., 2023). **DINOv2** (Oquab et al., 2023) is capable of extracting robust visual features for various downstream tasks and is particularly effective at capturing fine-grained local information (Tong et al., 2024b). Consequently, prior works (Liu et al., 2023; Zhang et al., 2024) leverage DINOv2 to match dense points of target objects under few-shot settings. **SAM** (Kirillov et al., 2023) is a promptable segmentation model that demonstrates strong generalization potential in both Cross-Domain Segmentation (Xiao et al., 2024a;b) and Few-Shot Segmentation (Zhang et al., 2023; Liu et al., 2023; Zhang et al., 2024) tasks. It is composed of three main components: an image encoder, a prompt encoder, and a mask decoder (as illustrated in Fig. 1(a)).

3.2. Influence of Prompt Point Density

To further validate our assumption in Sec. 1 that prompt point density influences segmentation performance, we conduct comprehensive experiments on both in-domain (*i.e.*, COCO-20i (Nguyen & Todorovic, 2019)) and cross-domain (*i.e.*, ISIC (Codella et al., 2019; Tschandl et al., 2018) and DeepGlobe (Demir et al., 2018)) datasets. Specifically, we place uniformly sampled points with varying densities on reference images and retain only those within the reference masks as prompt points, which are then fed into SAM for segmentation. As shown in Fig. 3, the in-domain dataset

exhibits robust performance across different prompt point densities, whereas cross-domain datasets are more sensitive and suffer significant performance drop when dense points are used. Moreover, we observe that different categories achieve their best performance under different prompt point densities, indicating that a fixed density is suboptimal. For example, although most categories attain optimal performance with low-density points, some categories, such as *nevus* in ISIC and *cd*, *pad*, and *bucket* in COCO-20i, achieve their best performance with medium- or high-density points. These observations motivate the need for an adaptive mechanism to regulate prompt point density, leading us to propose CPS, which adaptively sparsifies prompt points, particularly for cross-domain scenarios.

3.3. Accuracy of Matched Points

In this paper, following previous work (Zhang et al., 2024), we obtain prompt points on the target image via a dense matching strategy, which is described in detail in Sec. 4.1. This strategy yields highly accurate prompt points on the target images, as analyzed in the appendix. These observations further suggest that the limitations of existing methods mainly lie in SAM’s point–image interaction, while the densely matched points provide a reliable initialization for our proposed method.

3.4. Task Formulation

Cross-Domain Few-Shot Segmentation (CD-FSS) aims to segment target objects in a cross-domain image conditioned on a few reference images. In this paper, we address the CD-FSS task in a training-free manner by leveraging the strong generalization capability of visual foundation models (Kirillov et al., 2023; Oquab et al., 2023). Consequently, the task involves only an inference stage, and the problem setting can be simplified as follows. For each task, a reference image set $R = \{(I_i^r, M_i^r)\}_{i=1}^K$ is provided, which consists of K reference images $\{I_i^r\}_{i=1}^K$ and corresponding segmentations masks $\{M_i^r\}_{i=1}^K$, along with a target image I^t . The goal is to predict an accurate segmentation mask M^t of I^t , where the target object belongs to the same category as that specified in the reference image set R .

4. Method

We describe our proposed Conditional Point Sparsification (CPS) in this section, which aims to provide suitable prompt points for SAM under the challenging Cross-Domain Few-Shot Segmentation (CD-FSS) task. The overall pipeline of CPS consists of four steps as illustrated in Fig. 4: (i) dense point matching between the reference image I^r and the target image I^t , followed by boundary point pruning to obtain an initial set of prompt points \tilde{P}^t for segmentation (Sec. 4.1); (ii) sparsification of the dense point set \tilde{P}^t on

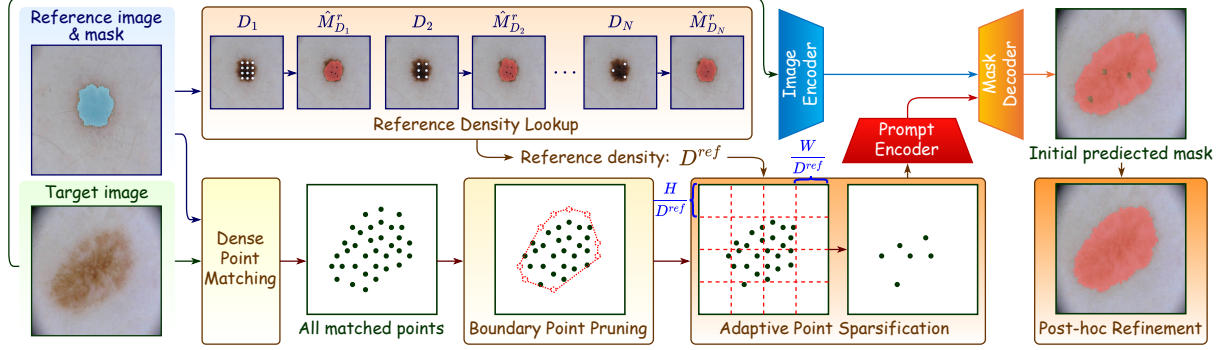


Figure 4. Overview of the proposed Conditional Point Sparsification (CPS). CPS not only leverages the reference image to match candidate prompt points in the target image (Sec. 4.1), but also exploits the reference image to determine an appropriate point density for subsequent sparsification (Sec. 4.3). The proposed modules, including boundary point pruning (Sec. 4.1), adaptive point sparsification (Sec. 4.2), and post-hoc mask refinement (Sec. 4.4), jointly contribute to producing accurate segmentation masks of the target image.

the target image to reduce ambiguity while preserving representative structural cues (Sec. 4.2); (iii) reference point density lookup on the reference image I^r , which provides a conditional density signal to guide the sparsification process and is subsequently used to predict the initial segmentation mask \hat{M}^t (Sec. 4.3); and (iv) post-hoc refinement of the \hat{M}^t and generation of the final mask \tilde{M}^t (Sec. 4.4).

4.1. Dense Point Matching and Boundary Point Pruning

We first introduce the **Dense Point Matching** design for obtaining an initial set of prompt points, which serves as a proper initialization for the subsequent sparsification stage. The core idea is to exploit the correspondence between the reference image I^r and the target image I^t to identify candidate regions. To this end, we adopt the Positive-Negative Alignment (PNA) module proposed in prior work (Zhang et al., 2024) to perform support-query alignment. Specifically, PNA employs DINOv2 (Oquab et al., 2023) as the visual encoder to extract image features:

$$F^r = \text{DINOv2}(I^r), \quad F^t = \text{DINOv2}(I^t), \quad (1)$$

where $F^r \in \mathbb{R}^{h \times w}$ and $F^t \in \mathbb{R}^{h \times w}$ denote the feature maps of the reference image $I^r \in \mathbb{R}^{H \times W}$ and the target image $I^t \in \mathbb{R}^{H \times W}$, respectively. PNA then establishes dense correspondences between F^r and F^t by jointly utilizing foreground and background regions to consider global and local similarities, yielding a set of matched points on the target feature map F^t . Further implementation details are provided in the appendix. For simplicity, we denote the resulting matched point set as:

$$\mathbf{p}^t = \{p_l^t\}_{l=1}^N = \text{PNA}(F^r, F^t), \quad (2)$$

where each matched point is parameterized as $p_l^t = (x_l^t, y_l^t)$ with $x_l^t \in \{0, \dots, w-1\}$ and $y_l^t \in \{0, \dots, h-1\}$. Here, p_l^t denotes the l -th matched point on the target feature map F^t , and \mathbf{p}^t represents a set of N candidate target points that are highly likely to fall within the target region. Since

each point $p_l^t \in \mathbf{p}^t$ is defined on the DINOv2 feature map of dimension $h \times w$, whereas SAM (Kirillov et al., 2023) expects prompt points in the image space with input resolution $H \times W$, we project each point into the SAM input space. For each matched point $p_l^t = (x_l^t, y_l^t)$ on the feature map, its corresponding coordinate $P_l^t = (X_l^t, Y_l^t)$ in the SAM input space is computed as:

$$X_l^t = \left(x_l^t + \frac{1}{2} \right) \cdot \frac{W}{w}, \quad Y_l^t = \left(y_l^t + \frac{1}{2} \right) \cdot \frac{H}{h}, \quad (3)$$

where the half-grid offset ensures that each projected point is aligned with the center of the corresponding image region. The resulting projected point set is:

$$\mathbf{P}^t = \{P_l^t\}_{l=1}^N, \quad (4)$$

which lies in the same spatial domain as the SAM encoder and serves as the input for subsequent sparsification (refer to Sec. 3.3). However, this linear coordinate mapping may introduce spatial misalignment due to the resolution discrepancy between the feature map and the original image. Consequently, some projected points may be shifted toward boundary regions or even fall into background areas, thereby introducing unreliable prompts for SAM.

To mitigate these potential issues, we first propose a **Boundary Point Pruning** strategy.¹ Specifically, given the mapped point set \mathbf{P}^t , we compute its convex hull (De Berg et al., 2008) to approximate the coarse spatial extent of the target object. Formally, let:

$$\mathcal{H}^t = \text{ConvexHull}(\mathbf{P}^t) \quad (5)$$

denote the convex hull of the mapped points, and let $\mathcal{V}(\mathcal{H}^t)$ represent the set of vertices of \mathcal{H}^t . Points lying on the convex hull boundary are more likely to be affected by spatial misalignment and background interference. Therefore, we

¹For clarity, we describe the scenario with a single target object in this section. The extension to images containing multiple target objects is discussed in the appendix.

remove these boundary points and retain only the interior points for subsequent processing:

$$\tilde{\mathbf{P}}^t = \{P_l^t \in \mathbf{P}^t \mid P_l^t \notin \mathcal{V}(\mathcal{H}^t)\}. \quad (6)$$

This operation effectively suppresses potentially noisy prompt points near object boundaries, yielding a more reliable prompt point set. Based on this refined set, we further perform point sparsification on $\tilde{\mathbf{P}}^t$ in Sec. 4.2.

4.2. Adaptive Point Sparsification

As discussed in Sec. 1 and Sec. 3, although the dense point set $\tilde{\mathbf{P}}^t$ obtained in Sec. 4.1 provides a strong initialization, it is not suitable for CD-FSS. Specifically, significant discrepancies in visual patterns across domains prevent these dense points from serving as reliable prompts for cross-domain images. Moreover, excessively dense points tend to introduce ambiguity in target object segmentation. Therefore, it is necessary to sparsify the prompt points while preserving their structural representativeness.

A straightforward yet effective strategy is to sparsify points region-wise using a uniform grid. Specifically, we select an adaptive sparsification density D^t (determined in Sec. 4.3) and partition the target image into a regular grid of $D^t \times D^t$ cells. Let:

$$\Delta_h^t = \frac{H}{D^t}, \quad \Delta_w^t = \frac{W}{D^t} \quad (7)$$

denote the cell height and width, respectively. Each grid cell is indexed by (i, j) , where $i, j \in \{0, 1, \dots, D^t - 1\}$, and corresponds to the spatial region:

$$\mathcal{G}_{i,j} = [i\Delta_h^t, (i+1)\Delta_h^t) \times [j\Delta_w^t, (j+1)\Delta_w^t). \quad (8)$$

To select a representative point from each cell, we first compute the global centroid of all remaining points $\tilde{\mathbf{P}}^t$:

$$C = \frac{1}{|\tilde{\mathbf{P}}^t|} \sum_{\tilde{P}^t \in \tilde{\mathbf{P}}^t} \tilde{P}^t, \quad (9)$$

which approximates the central location of the target object in the image space. For each grid cell $\mathcal{G}_{i,j}$, we collect all points from $\tilde{\mathbf{P}}^t$ that fall inside the cell:

$$\tilde{\mathbf{P}}_{i,j}^t = \left\{ \tilde{P}^t \in \tilde{\mathbf{P}}^t \mid \tilde{P}^t \in \mathcal{G}_{i,j} \right\}. \quad (10)$$

If $\tilde{\mathbf{P}}_{i,j}^t$ is non-empty, we retain only the point closest to the global centroid C :

$$P_{i,j}^* = \arg \min_{\tilde{P}_{i,j}^t \in \tilde{\mathbf{P}}_{i,j}^t} \left\| \tilde{P}_{i,j}^t - C \right\|_2. \quad (11)$$

The region-level sparsified point set is then obtained by aggregating the selected points from all grid cells:

$$\hat{\mathbf{P}}^t = \bigcup_{i,j} P_{i,j}^*. \quad (12)$$

By selecting points that are spatially distributed via grid partitioning, this strategy reduces the density of the $\tilde{\mathbf{P}}^t$ while preserving the structural cues of the target object.

4.3. Conditional Design

As discussed in Sec. 3.2, different datasets and object categories exhibit optimal segmentation performance under different prompt point densities. Inspired by prior works (Liu et al., 2023; Zhang et al., 2024) that utilize the reference image for point matching, we further exploit the reference image as a reliable exemplar to determine an appropriate point density D^{ref} for sparsification in Sec. 4.2, rather than using a manually defined density.

First, we introduce the **Reference Density Lookup** design, which identifies a suitable point density from a set of candidate densities $\mathbf{D} = \{D_1, D_2, \dots, D_N\}$. For each density $D_i \in \mathbf{D}$, we uniformly sample prompt points on the reference image $I^r \in \mathbb{R}^{H \times W}$ using a regular grid. The sampling interval along the height and width is computed as:

$$\Delta_h^r = \frac{H}{D_i}, \quad \Delta_w^r = \frac{W}{D_i}. \quad (13)$$

The resulting set of grid points is:

$$\mathbf{P}_{D_i}^r = \{(m\Delta_h^r, n\Delta_w^r) \mid m, n \in \{0, 1, \dots, D_i\}\}. \quad (14)$$

We then retain only the points that fall within the foreground region, where $M^r(\cdot) = 1$. Formally, the filtered point set is:

$$\tilde{\mathbf{P}}_{D_i}^r = \{P_{D_i}^r \in \mathbf{P}_{D_i}^r \mid M^r(P_{D_i}^r) = 1\}. \quad (15)$$

These retained points $\tilde{\mathbf{P}}_{D_i}^r$ are then used as prompts for SAM to predict a segmentation mask on the reference image:

$$\hat{M}_{D_i}^r = \text{SAM}(I^r, \tilde{\mathbf{P}}_{D_i}^r). \quad (16)$$

Next, we evaluate the quality of each density D_i using the Intersection over Union (IoU) between the predicted mask $\hat{M}_{D_i}^r$ and the ground-truth mask M^r :

$$\text{IoU}(D_i) = \frac{|\hat{M}_{D_i}^r \cap M^r|}{|\hat{M}_{D_i}^r \cup M^r|}. \quad (17)$$

Finally, we select the density D_i that yields the highest mIoU as the reference density D^{ref} :

$$D^{ref} = \arg \max_{D_i \in \mathbf{D}} \text{mIoU}(D_i). \quad (18)$$

The selected conditional density D^{ref} then replaces the D^t in Eq. 7, enabling **Adaptive Point Sparsification** of $\hat{\mathbf{P}}^t$ on the target image as described in Sec. 4.2, resulting in the sparsified point set $\hat{\mathbf{P}}^t$. The $\hat{\mathbf{P}}^t$ is then used to generate an initial segmentation mask for I^t via SAM:

$$\hat{M}^t = \text{SAM}(I^t, \hat{\mathbf{P}}^t). \quad (19)$$

Table 1. Quantitative comparisons between the proposed CPS and existing methods over four widely adopted Cross-Domain Few-Shot Segmentation benchmarks (in mIoU (%)). The best mIoU number under each setup is highlighted by **bold** font.

Method	ISIC		Chest X-Ray		DeepGlobe		SUIM	
	1-shot	5-shot	1-shot	5-shot	1-shot	5-shot	1-shot	5-shot
<i>Training-required Methods</i>								
RPMMS	18.0	20.0	30.1	30.8	13.0	13.5	-	-
PGNet	21.9	21.3	34.0	28.0	10.7	12.4	-	-
RePRI	23.3	26.2	65.1	65.5	25.0	27.4	-	-
PFENet	23.5	23.8	27.2	27.6	16.9	18.0	-	-
PANet	25.3	34.0	57.8	69.3	36.6	45.3	-	-
CaNet	25.2	28.2	28.4	28.6	22.3	23.1	-	-
AMP	28.4	30.4	51.2	53.0	37.6	40.6	-	-
HSNet	31.2	35.1	51.9	54.4	29.7	35.1	28.8	-
PATNet	41.2	53.6	66.6	70.2	37.9	43.0	32.1	40.2
ABCDFSS	45.7	53.3	79.8	81.4	42.6	49.0	35.1	41.3
SSP	48.6	65.4	72.6	73.0	41.3	54.2	-	-
<i>SAM-based Training-free Methods</i>								
PerSAM	23.9	-	-	-	31.4	-	-	-
Matcher	38.6	35.0	66.8	66.3	48.1	50.9	37.9	41.4
GF-SAM	48.7	55.2	47.6	47.4	49.5	57.7	38.3	42.9
CPS	51.3	56.6	70.0	70.2	46.0	49.8	42.8	48.8

4.4. Post-hoc Mask Refinement

As shown in Fig. 1, the activation heatmap induced by prompt points may exhibit discontinuous patterns. Such discontinuities can result in unexpected holes within the target region or abrupt changes along object boundaries when SAM applies a fixed threshold (Kirillov et al., 2023; Liu et al., 2023; Zhang et al., 2024) to generate the segmentation mask. To address this issue, we propose a post-hoc refinement strategy to regularize the initial predicted mask.

Specifically, we employ morphological opening and closing operations (Serra, 1982) to suppress isolated activations and fill small holes, thereby enforcing spatial continuity and improving boundary smoothness. Formally, $\hat{M}^t \in \mathbb{R}^{H \times W}$ denotes the initial predicted mask of the target image from Sec. 4.2, and let K be a morphological structuring element. The refined prediction map \tilde{M}^t is obtained by sequentially applying opening and closing operations:

$$\tilde{M}^t = (\hat{M}^t \circ K) \bullet K, \quad (20)$$

where \circ and \bullet represent morphological opening and closing, respectively. The opening operation removes small isolated activations, while the closing operation fills small gaps and holes, resulting in a more spatially coherent predicted mask.

5. Experiment

5.1. Datasets

We conduct extensive experiments on four cross-domain datasets spanning medical images (Codella et al., 2019; Tschandl et al., 2018; Candemir et al., 2013; Jaeger et al., 2013), satellite images (Demir et al., 2018), and underwater

scenes (Islam et al., 2020). **ISIC2018** (Codella et al., 2019; Tschandl et al., 2018) consists of images for skin lesion analysis and covers three types of skin lesions. **Chest X-Ray** (Candemir et al., 2013; Jaeger et al., 2013) is collected for tuberculosis screening. The grayscale nature of this dataset further increases the diversity of evaluation domains. **DeepGlobe** (Demir et al., 2018) is a satellite image dataset containing six terrain categories, including urban, agriculture, rangeland, forest, water, and barren areas. Following PATNet (Lei et al., 2022), we split the original images into smaller patches for the Cross-Domain Few-Shot Segmentation (CD-FSS) setting. **SUIM** (Islam et al., 2020) is an underwater image dataset comprising seven object categories, including fish, plants, divers, robots, ruins, and rocks.

5.2. Implementation Details

Following the experimental settings of Matcher (Liu et al., 2023) and GF-SAM (Xu et al., 2024) for fair comparison, we adopt DINOv2 (Oquab et al., 2023) with a ViT-L/14 backbone (Dosovitskiy, 2020) to perform dense point matching and generate candidate prompt points. These points are refined by the proposed Boundary Point Pruning and Adaptive Point Sparsification modules. The remaining prompt points, together with the target image, are then fed into SAM (Kirillov et al., 2023) with a ViT-H backbone (Dosovitskiy, 2020) to produce segmentation masks. Following Matcher and GF-SAM, the input image resolution is set to 518×518 for DINOv2 and 1024×1024 for SAM. We evaluate the segmentation performance using the mean Intersection over Union (mIoU) metric. All experiments are conducted on a single NVIDIA RTX 4090 GPU.

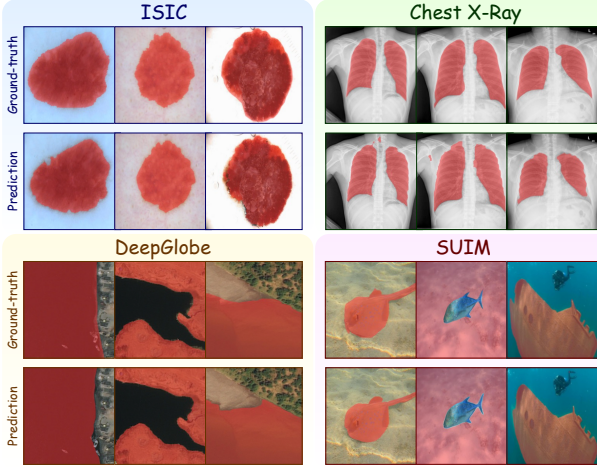


Figure 5. Qualitative segmentation results (red mask) of CPS on samples from four Cross-Domain Few-Shot Segmentation datasets. More examples are provided in the appendix.

5.3. Comparison of Performance on CD-FSS Datasets

We evaluate our proposed Conditional Point Sparsification (CPS) on four representative CD-FSS datasets and compare it with two groups of state-of-the-art methods in Tab. 1. Overall, CPS consistently achieves superior performance across most subsets, often by a large margin. We first compare CPS with traditional CD-FSS methods (Yang et al., 2020; Zhang et al., 2019a; Boudiaf et al., 2021; Tian et al., 2020; Wang et al., 2019; Zhang et al., 2019b; Siam et al., 2019; Min et al., 2021; Lei et al., 2022; Herzog, 2024; Fan et al., 2022), which are typically built upon relatively small backbones (*e.g.*, ResNet-50 (He et al., 2016)) and rely on task-specific training and fine-tuning. Despite being completely training-free, CPS demonstrates competitive or superior performance compared to these training-dependent approaches. Due to the high computational cost and limited cross-domain generalization of training-based pipelines, recent works have shifted toward either adaptation-only strategies (Herzog, 2024) or training-free methods that leverage the strong generalization ability of SAM (Kirillov et al., 2023) (Zhang et al., 2023; Liu et al., 2023; Zhang et al., 2024). We further benchmark CPS against these training-free SAM-based methods and observe consistent improvements, validating the effectiveness of our proposed point sparsification and refinement strategies.

From a performance perspective, MPA consistently delivers strong results across diverse domains, including medical imaging, remote sensing, and underwater scenes, demonstrating its robustness and cross-domain generalization capability. The medical images in ISIC (Codella et al., 2019; Tschandl et al., 2018) and Chest X-Ray (Candemir et al., 2013; Jaeger et al., 2013) exhibit relatively clean backgrounds, with target regions occupying a large portion of the image. As analyzed in Fig. 2, the target regions demonstrate

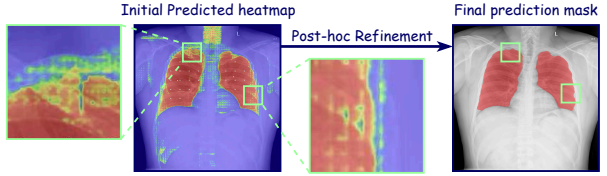


Figure 6. Illustrative example of Post-hoc Mask Refinement.

Table 2. Ablation studies for technical designs of CPS. The Conditional Point Sparsification, Boundary Point Pruning, and Post-hoc Mask Refinement designs show significant effectiveness.

Incorporated design	ISIC	SUIM
Baseline	39.3	34.2
+Adaptive Point Sparsification	47.2	40.6
+Boundary Point Pruning	47.7	41.2
+Post-hoc Mask Refinement	51.3	42.8

high intra-mask feature consistency, under which our point sparsification strategy performs particularly well. Specifically, it surpasses state-of-the-art SAM-based methods by 2.6% and 3.2% on ISIC and Chest X-Ray, respectively. For the underwater images in SUIM (Islam et al., 2020), the background also contains multiple semantic objects, leading to a more complex and cluttered visual context. Nevertheless, CPS still achieves a new state-of-the-art performance, outperforming existing methods by 4.5% under the 1-shot setup. DeepGlobe (Demir et al., 2018) is characterized by an aerial viewpoint and a highly complex background. Although its intra-mask feature consistency is higher than that of medical images (see Fig. 2), CPS still achieves competitive performance on this dataset. Moreover, it is worth noting that CPS consistently achieves better performance in the 5-shot setting than in the 1-shot setting, indicating that this training-free approach can leverage more informative prompts when additional support images are provided. In addition, we conduct qualitative comparisons on multiple CD-FSS datasets to further demonstrate the effectiveness of CPS. As shown in Fig. 5, CPS produces accurate and coherent segmentation masks.

From an efficiency perspective, CPS not only outperforms methods that require training or fine-tuning (Lei et al., 2022; Herzog, 2024), but also demonstrates higher efficiency than some SAM-based approaches (Liu et al., 2023). More details are provided in the appendix.

5.4. Discussion

Technical design ablation. We conduct ablation studies to evaluate the effectiveness of the proposed Boundary Point Pruning (Sec. 4.1), Adaptive Point Sparsification (Sec. 4.2 and Sec. 4.3), and Post-hoc Mask Refinement (Sec. 4.4) modules. As a baseline, we directly use all densely matched points obtained in Sec. 4.1 as input prompts for SAM. As

Table 3. Quantitative comparisons between the proposed CPS and existing methods over two widely adopted natural image Few-Shot Segmentation benchmarks (in mIoU (%)). The best mIoU number under each setup is highlighted by **bold** font.

Method	COCO-20i										Method	FSS-1000		
	1-shot					5-shot						1-shot	5-shot	
	20 ⁰	20 ¹	20 ²	20 ³	Avg.	20 ⁰	20 ¹	20 ²	20 ³	Avg.				
SSP	35.5	39.6	37.9	36.7	37.4	40.6	47.0	45.1	43.9	44.1	RePRI	71.0	74.2	
CyCTR	38.9	43.0	39.6	39.8	40.3	41.1	48.9	45.2	47.0	45.6	ABCDfSS	74.6	76.2	
HSNet	37.2	44.1	42.4	41.3	41.2	45.9	53.0	51.8	47.1	49.5	SSP	77.0	79.4	
BAM	43.4	50.6	47.5	43.4	46.2	49.3	54.2	51.6	49.6	51.2	HSNet	77.5	81.0	
PAM	44.1	55.0	46.5	48.5	48.5	48.1	60.8	54.8	51.9	53.9	PATNet	78.6	81.2	
AENet	43.1	56.0	50.3	48.4	49.4	51.7	61.9	57.9	55.3	56.7	DR-Adapter	79.1	80.4	
HDMNet	44.8	54.9	50.0	48.7	49.6	50.9	60.2	55.0	55.3	55.3	IFA	80.1	82.4	
PerSAM	-	-	-	-	23.0	-	-	-	-	-	PerSAM	71.2	-	
PerSAM-F	-	-	-	-	23.5	-	-	-	-	-	PerSAM-F	75.6	-	
CPS	46.3	52.6	48.2	49.6	49.2	52.5	56.2	53.1	65.7	56.9	CPS	81.7	82.8	

Table 4. Effectiveness of Boundary Point Pruning in improving point accuracy. The accuracy represents the ratio of points that fall within the ground-truth masks of the target images.

Setup	ISIC	Chest X-Ray
Accuracy of all matched points	77.2	94.7
Accuracy after Boundary Point Pruning	81.4	96.9

reported in Tab. 2, this baseline yields unsatisfactory performance, indicating that although the matched points are relatively accurate (see Sec. 3.3), directly using dense points is not suitable for CD-FSS tasks. We then incorporate the core design, **Adaptive Point Sparsification**, which adaptively reduces the point density on the target image conditioned on the reference density derived from the reference image. This results in substantial performance improvements of 7.9% and 6.4% on the two evaluated datasets. Next, we further introduce **Boundary Point Pruning** to remove points that are more likely to fall into background regions, leading to additional gains of 0.5% and 0.6%, respectively. Finally, applying the proposed **Post-hoc Mask Refinement** module brings further improvements of 3.6% and 1.6% on the two datasets. These results demonstrate that each component contributes positively to the overall performance, and their combination yields the best results.

Effectiveness of Boundary Point Pruning. As shown in Tab. 4, Boundary Point Pruning improves the accuracy of matched points on two datasets. This indicates that this strategy filters out some inaccurately matched points, thereby providing more reliable prompts for segmentation.

Illustrative example of Post-hoc Mask Refinement. As shown in Fig. 6, the refinement process effectively improves the final predictions, particularly by enforcing spatial continuity and enhancing boundary smoothness.

Point sparsification strategies. We compare a fixed density sparsification strategy with the proposed Adaptive Point Sparsification in Tab. 5. Specifically, the fixed density strat-

Table 5. Comparison between our designed Adaptive Point Sparsification and fixed density sparsification.

Incorporated design	ISIC	SUIM
Baseline	39.3	34.2
+Fixed Density Sparsification ($D = 4$)	46.2	36.1
+Fixed Density Sparsification ($D = 8$)	44.5	38.8
+Fixed Density Sparsification ($D = 12$)	41.8	38.2
+Adaptive Point Sparsification	47.2	40.6

egy adopts a manually defined point density as guidance, instead of adaptively selecting the density conditioned on the reference image. As a result, it achieves only limited improvements over the baseline and consistently underperforms our adaptive strategy. These results further validate the importance of adaptively determining an appropriate point density for each target image.

5.5. Generalization Potential of CPS

We also evaluate the proposed CPS on two in-domain datasets consisting of natural images that are similar to the training data of SAM (Kirillov et al., 2023). Specifically, we select **FSS-1000**² (Li et al., 2020), which comprises natural images of everyday objects, and the more challenging **COCO-20i** (Nguyen & Todorovic, 2019), which covers 80 classes with complex and cluttered background. Both datasets contain tiny objects, enabling us to examine whether sparse points introduce negative effects. As shown in Tab. 3, our proposed CPS achieves competitive performance on both datasets. More detailed analysis and qualitative segmentation results are provided in the appendix.

²FSS-1000 is regarded as a “cross-domain” dataset in prior CD-FSS works, as they adopt ImageNet-pretrained backbones whose training distribution differs from FSS-1000. In contrast, for SAM-based methods (Liu et al., 2023; Zhang et al., 2024), FSS-1000 is considered an “in-domain” dataset because it consists of natural images that largely fall within the training distribution of SAM.

6. Conclusion

In this work, we investigate the challenges of applying dense prompt points in Cross-Domain Few-Shot Segmentation (CD-FSS), where large domain shifts significantly impair SAM’s mask prediction. We identify that point density plays a crucial role under such cross-domain conditions and propose Conditional Point Sparsification (CPS), a training-free method that adaptively guides SAM interactions based on reference exemplars. By leveraging ground-truth masks to appropriately sparsify dense matched points, CPS ensures more reliable and accurate segmentation across diverse domains. Extensive experiments on multiple CD-FSS datasets demonstrate that CPS outperforms existing training-free SAM-based approaches, validating the effectiveness of our designs in handling domain shifts. Overall, our study highlights the importance of carefully controlling prompt points in cross-domain scenarios and provides a practical solution for extending SAM’s capabilities to challenging CD-FSS segmentation tasks.

References

Boudiaf, M., Kervadec, H., Masud, Z. I., Piantanida, P., Ben Ayed, I., and Dolz, J. Few-shot segmentation without meta-learning: A good transductive inference is all you need? In *CVPR*, 2021.

Candemir, S., Jaeger, S., Palaniappan, K., Musco, J. P., Singh, R. K., Xue, Z., Karargyris, A., Antani, S., Thoma, G., and McDonald, C. J. Lung segmentation in chest radiographs using anatomical atlases with nonrigid registration. *TMI*, 2013.

Chen, H., Dong, Y., Lu, Z., Yu, Y., and Han, J. Pixel matching network for cross-domain few-shot segmentation. In *WACV*, 2024a.

Chen, J., Quan, R., and Qin, J. Cross-domain few-shot semantic segmentation via doubly matching transformation. In *IJCAI*, 2024b.

Chen, T., Zhu, L., Ding, C., Cao, R., Wang, Y., Li, Z., Sun, L., Mao, P., and Zang, Y. Sam fails to segment anything?—sam-adapter: Adapting sam in underperformed scenes: Camouflage, shadow, medical image segmentation, and more. *arXiv preprint arXiv:2304.09148*, 2023.

Codella, N., Rotemberg, V., Tschandl, P., Celebi, M. E., Dusza, S., Gutman, D., Helba, B., Kalloo, A., Liopyris, K., Marchetti, M., et al. Skin lesion analysis toward melanoma detection 2018: A challenge hosted by the international skin imaging collaboration (isic). *arXiv preprint arXiv:1902.03368*, 2019.

Cuttano, C., Trivigno, G., Averta, G., and Masone, C. Sansa: Unleashing the hidden semantics in SAM2 for few-shot segmentation. In *NeurIPS*, 2025.

De Berg, M., Cheong, O., Van Kreveld, M., and Overmars, M. *Computational geometry: algorithms and applications*. Springer, 2008.

Demir, I., Koperski, K., Lindenbaum, D., Pang, G., Huang, J., Basu, S., Hughes, F., Tuia, D., and Raskar, R. Deepglobe 2018: A challenge to parse the earth through satellite images. In *CVPRW*, 2018.

Deng, J., Dong, W., Socher, R., Li, L.-J., Li, K., and Fei-Fei, L. Imagenet: A large-scale hierarchical image database. In *CVPR*, 2009.

Ding, L., Zhu, K., Peng, D., Tang, H., Yang, K., and Bruzzone, L. Adapting segment anything model for change detection in vhr remote sensing images. *TGRS*, 2024.

Dosovitskiy, A. An image is worth 16x16 words: Transformers for image recognition at scale. In *ICLR*, 2020.

Fan, H., Fan, Q., Pagnucco, M., and Song, Y. Darnet: Bridging domain gaps in cross-domain few-shot segmentation with dynamic adaptation. *arXiv preprint arXiv:2312.04813*, 2023.

Fan, Q., Pei, W., Tai, Y.-W., and Tang, C.-K. Self-support few-shot semantic segmentation. In *ECCV*, 2022.

Fan, Q., Liu, K., Liu, N., Cholakkal, H., Anwer, R. M., Li, W., and Gao, Y. Adapting in-domain few-shot segmentation to new domains without retraining. *arXiv preprint arXiv:2504.21414*, 2025.

Fang, H., Grotz, M., Pumacay, W., Wang, Y. R., Fox, D., Krishna, R., and Duan, J. Sam2act: Integrating visual foundation model with a memory architecture for robotic manipulation. In *ICML*, 2025.

Fu, Y., Wang, Y., Pan, Y., Huai, L., Qiu, X., Shangguan, Z., Liu, T., Fu, Y., Van Gool, L., and Jiang, X. Cross-domain few-shot object detection via enhanced open-set object detector. In *ECCV*, 2024.

He, K., Zhang, X., Ren, S., and Sun, J. Deep residual learning for image recognition. In *CVPR*, 2016.

He, W., Zhang, Y., Zhuo, W., Shen, L., Yang, J., Deng, S., and Sun, L. Apseg: Auto-prompt network for cross-domain few-shot semantic segmentation. In *CVPR*, 2024.

Herzog, J. Adapt before comparison: A new perspective on cross-domain few-shot segmentation. In *CVPR*, 2024.

Huang, X., Zhu, C., and Chen, W. Restnet: Boosting cross-domain few-shot segmentation with residual transformation network. In *BMVC*, 2023.

Islam, M. J., Edge, C., Xiao, Y., Luo, P., Mehtaz, M., Morse, C., Enan, S. S., and Sattar, J. Semantic segmentation of underwater imagery: Dataset and benchmark. In *IROS*, 2020.

Jaeger, S., Karargyris, A., Candemir, S., Folio, L., Siegelman, J., Callaghan, F., Xue, Z., Palaniappan, K., Singh, R. K., Antani, S., et al. Automatic tuberculosis screening using chest radiographs. *TMI*, 2013.

Ke, L., Ye, M., Danelljan, M., Tai, Y.-W., Tang, C.-K., Yu, F., et al. Segment anything in high quality. In *NeurIPS*, 2023.

Kirillov, A., Mintun, E., Ravi, N., Mao, H., Rolland, C., Gustafson, L., Xiao, T., Whitehead, S., Berg, A. C., Lo, W.-Y., et al. Segment anything. In *ICCV*, 2023.

Lang, C., Cheng, G., Tu, B., Li, C., and Han, J. Base and meta: A new perspective on few-shot segmentation. *TPAMI*, 2023.

Lei, S., Zhang, X., He, J., Chen, F., Du, B., and Lu, C.-T. Cross-domain few-shot semantic segmentation. In *ECCV*, 2022.

Li, K., Liu, R., Cao, X., Bai, X., Zhou, F., Meng, D., and Wang, Z. Segearth-ov: Towards training-free open-vocabulary segmentation for remote sensing images. In *CVPR*, 2025.

Li, X., Wei, T., Chen, Y. P., Tai, Y.-W., and Tang, C.-K. Fss-1000: A 1000-class dataset for few-shot segmentation. In *CVPR*, 2020.

Lin, T.-Y., Maire, M., Belongie, S., Hays, J., Perona, P., Ramanan, D., Dollár, P., and Zitnick, C. L. Microsoft coco: Common objects in context. In *ECCV*. Springer, 2014.

Liu, N., Xu, X., Su, Y., Zhang, H., and Li, H.-C. Pointsam: Pointly-supervised segment anything model for remote sensing images. *TGRS*, 2025.

Liu, Y., Zhu, M., Li, H., Chen, H., Wang, X., and Shen, C. Matcher: Segment anything with one shot using all-purpose feature matching. In *ICLR*, 2023.

Lu, Z., He, S., Zhu, X., Zhang, L., Song, Y.-Z., and Xiang, T. Simpler is better: Few-shot semantic segmentation with classifier weight transformer. In *ICCV*, 2021.

Ma, J., He, Y., Li, F., Han, L., You, C., and Wang, B. Segment anything in medical images. *Nature Communications*, 2024.

Maaten, L. v. d. and Hinton, G. Visualizing data using t-sne. *JMLR*, 2008.

Mazurowski, M. A., Dong, H., Gu, H., Yang, J., Konz, N., and Zhang, Y. Segment anything model for medical image analysis: an experimental study. *Medical Image Analysis*, 2023.

Min, J., Kang, D., and Cho, M. Hypercorrelation squeeze for few-shot segmentation. In *ICCV*, 2021.

Nguyen, K. and Todorovic, S. Feature weighting and boosting for few-shot segmentation. In *ICCV*, 2019.

Nie, J., Xing, Y., Zhang, G., Yan, P., Xiao, A., Tan, Y.-P., Kot, A. C., and Lu, S. Cross-domain few-shot segmentation via iterative support-query correspondence mining. In *CVPR*, 2024.

Oquab, M., Darabet, T., Moutakanni, T., Vo, H., Szafraniec, M., Khalidov, V., Fernandez, P., Haziza, D., Massa, F., El-Nouby, A., et al. Dinov2: Learning robust visual features without supervision. *arXiv preprint arXiv:2304.07193*, 2023.

Pan, M., Zhang, J., Wu, T., Zhao, Y., Gao, W., and Dong, H. Omnimaniip: Towards general robotic manipulation via object-centric interaction primitives as spatial constraints. In *CVPR*, 2025.

Ravi, N., Gabeur, V., Hu, Y.-T., Hu, R., Ryali, C., Ma, T., Khedr, H., Rädl, R., Rolland, C., Gustafson, L., et al. Sam 2: Segment anything in images and videos. *arXiv preprint arXiv:2408.00714*, 2024.

Rombach, R., Blattmann, A., Lorenz, D., Esser, P., and Ommer, B. High-resolution image synthesis with latent diffusion models. In *CVPR*, 2022.

Serra, J. *Image Analysis and Mathematical Morphology*. 1982.

Siam, M., Oreshkin, B. N., and Jagersand, M. Amp: Adaptive masked proxies for few-shot segmentation. In *ICCV*, 2019.

Su, J., Fan, Q., Pei, W., Lu, G., and Chen, F. Domain-rectifying adapter for cross-domain few-shot segmentation. In *CVPR*, 2024.

Sun, Y., Chen, J., Zhang, S., Zhang, X., Chen, Q., Zhang, G., Ding, E., Wang, J., and Li, Z. Vrp-sam: Sam with visual reference prompt. In *CVPR*, 2024.

Tian, Z., Zhao, H., Shu, M., Yang, Z., Li, R., and Jia, J. Prior guided feature enrichment network for few-shot segmentation. *TPAMI*, 2020.

Tong, J., Zou, Y., Li, Y., and Li, R. Lightweight frequency masker for cross-domain few-shot semantic segmentation. In *NeurIPS*, 2024a.

Tong, J., Zou, Y., Chen, G., Li, Y., and Li, R. Self-disentanglement and re-composition for cross-domain few-shot segmentation. *arXiv preprint arXiv:2506.02677*, 2025.

Tong, P., Brown, E., Wu, P., Woo, S., IYER, A. J. V., Akula, S. C., Yang, S., Yang, J., Middepogu, M., Wang, Z., et al. Cambrian-1: A fully open, vision-centric exploration of multimodal llms. In *NeurIPS*, 2024b.

Tschandl, P., Rosendahl, C., and Kittler, H. The ham10000 dataset, a large collection of multi-source dermatoscopic images of common pigmented skin lesions. *Scientific Data*, 2018.

Wang, C., Li, D., Wang, S., Zhang, C., Wang, Y., Liu, Y., and Yang, G. Sammed: A medical image annotation framework based on large vision model. *arXiv preprint arXiv:2307.05617*, 3, 2023.

Wang, K., Liew, J. H., Zou, Y., Zhou, D., and Feng, J. Panet: Few-shot image semantic segmentation with prototype alignment. In *ICCV*, 2019.

Wang, W., Duan, L., Wang, Y., En, Q., Fan, J., and Zhang, Z. Remember the difference: Cross-domain few-shot semantic segmentation via meta-memory transfer. In *CVPR*, 2022.

Wu, J., Liu, X., Yin, X., Zhang, T., and Zhang, Y. Task-adaptive prompted transformer for cross-domain few-shot learning. In *AAAI*, 2024.

Wu, J., Wang, Z., Hong, M., Ji, W., Fu, H., Xu, Y., Xu, M., and Jin, Y. Medical sam adapter: Adapting segment anything model for medical image segmentation. *Medical image analysis*, 2025.

Xiao, A., Xuan, W., Qi, H., Xing, Y., Ren, R., Zhang, X., Shao, L., and Lu, S. Cat-sam: Conditional tuning for few-shot adaptation of segment anything model. In *ECCV*, 2024a.

Xiao, A., Xuan, W., Qi, H., Xing, Y., Yokoya, N., and Lu, S. Segment anything with multiple modalities. *arXiv preprint arXiv:2408.09085*, 2024b.

Xu, Q., Liu, X., Zhu, L., Lin, G., Long, C., Li, Z., and Zhao, R. Hybrid mamba for few-shot segmentation. In *NeurIPS*, 2024.

Xu, Q., Zhu, L., Liu, X., Lin, G., Long, C., Li, Z., and Zhao, R. Unlocking the power of sam 2 for few-shot segmentation. In *ICML*, 2025.

Yan, Z., Li, J., Li, X., Zhou, R., Zhang, W., Feng, Y., Diao, W., Fu, K., and Sun, X. Ringmo-sam: A foundation model for segment anything in multimodal remote-sensing images. *TGRS*, 2023.

Yang, B., Liu, C., Li, B., Jiao, J., and Ye, Q. Prototype mixture models for few-shot semantic segmentation. In *ECCV*, 2020.

Yang, J., Huang, Y., He, X., Shen, L., and Qiu, G. Tavp: Task-adaptive visual prompt for cross-domain few-shot segmentation. *arXiv preprint arXiv:2409.05393*, 2024.

Yang, M., Lu, J., and Kim, H.-S. Sam-guided pseudo label enhancement for multi-modal 3d semantic segmentation. *arXiv preprint arXiv:2502.00960*, 2025.

Zhang, A., Gao, G., Jiao, J., Liu, C., and Wei, Y. Bridge the points: Graph-based few-shot segment anything semantically. In *NeurIPS*, 2024.

Zhang, C., Lin, G., Liu, F., Guo, J., Wu, Q., and Yao, R. Pyramid graph networks with connection attentions for region-based one-shot semantic segmentation. In *ICCV*, 2019a.

Zhang, C., Lin, G., Liu, F., Yao, R., and Shen, C. Canet: Class-agnostic segmentation networks with iterative refinement and attentive few-shot learning. In *CVPR*, 2019b.

Zhang, R., Jiang, Z., Guo, Z., Yan, S., Pan, J., Ma, X., Dong, H., Gao, P., and Li, H. Personalize segment anything model with one shot. In *ICLR*, 2023.

Zhang, S., Wang, Q., Liu, J., and Xiong, H. Alps: An auto-labeling and pre-training scheme for remote sensing segmentation with segment anything model. *TIP*, 2025.

Zhu, M., Liu, Y., Luo, Z., Jing, C., Chen, H., Xu, G., Wang, X., and Shen, C. Unleashing the potential of the diffusion model in few-shot semantic segmentation. In *NeurIPS*, 2024.